Synthesis, spectroscopy, DFT and crystal structure investigations of 3-methoxy-2-hydroxybenzaldehyde S-ethylisothiosemicarbazone and its Ni(II) and Mo(VI) complexes

Reza Takjoo [a],*, Alireza Akbari [b],*, Mehdi Ahmadi [b], Hadi Amiri Rudbari [c], Giuseppe Bruno [d]

[a] Department of Chemistry, School of Sciences, Ferdowsi University of Mashhad, Mashhad 91775-1436, Iran
[b] Department of Chemistry, Payame Noor University (PNU), 19395-4697 Tehran, Iran
[c] Faculty of Chemistry, University of Isfahan, Isfahan 81746-73441, Iran
[d] Dipartimento di Chimica Inorganica, Chimica Analitica e Chimica Fisica, Università di Messina, Salita Sperone, 31 Contrada Papardo, 98166 Messina, Italy

ABSTRACT

Four new compounds, 3-methoxy-2-hydroxybenzaldehyde S-ethylisothiosemicarbazone (**H₂L**), (3-methoxy-2-hydroxybenzaldehyde S-ethyl-isothiosemicarbazonato-N,N′,O)-(1-methylimidazole)-nickel(II) (**1**), (3-methoxy-2-hydroxybenzaldehyde S-ethyl-isothiosemicarbazonato-N,N′,O)-(pyridine)-nickel(II) (**2**) and cis-dioxo-dimethylsulfoxide-(3-methoxy-2-hydroxybenzaldehyde S-ethyl-isothiosemicarbazonato-N,N′,O)-molybdenum(VI) (**3**), have been synthesized and characterized by molar conductivity, FT-IR, UV–Vis, ^{1}H NMR, elemental analysis and X-ray crystal structures. The crystal structure of **H₂L** reveals that the NH₂ and S–R moieties are in cis positions with respect to each other, and the molecule adopts the Z configuration. The ligand is bonded to the central metals as a binegatively tridentate agent. The Ni(II) atom adopts square planar geometry with this ligand, with the 1-methylimidazole and pyridine ligands occupying the remaining position in complexes **1** and **2** respectively. The Mo(VI) center in complex **3** is six coordinated by the ligand, two oxido groups and one DMSO molecule. The Density Functional Theory approach has been successfully used for the investigation of the ground state, frequency assignment and natural bond analysis.

© 2013 Elsevier Ltd. All rights reserved.

1. Introduction

There has been great interest in the research on thiosemicarbazones and transition metal complexes containing thiosemicarbazone since they have shown suitable applications in biological and analytical chemistry [1,2]. Also, a wide range of biological properties of isothiosemicarbazones and their metal complexes, such as antiviral [3], antimicrobial [4], antibacterial [5], cytotoxic [6] and antidiabetic [7] activities, have been mentioned. However, compared with thiosemicarbazones, the alkylated sulfur atom remains uncoordinated on complexation, and isothiosemicarbazones have shown different coordination modes. Recently, isothiosemicarbazones have attracted much consideration as template reaction precursors which cause an increase in the chelating sites for metal coordination [8]. A tridentate NNO isothiosemicarbazone donor ligand has the ability to participate in reactions in either the mono- or bi-negative form. These characteristics and proprieties make these compounds attractive for the preparation of a variety of new complexes [9–11].

Various properties of Ni(II) and Mo(VI) Schiff base complexes have been documented. It is well known that both of these metals have a big presence in coordination chemistry [12]. They have been shown to mimic biological sites and are used as catalysts in industrial processes. For the nickel(II) Schiff base complexes, different kinds of properties and applications, like anti-oxidation and polymerization of olefins, are demonstrated [13,14]. The molybdenum(VI) Schiff base complexes with a cis-MoO₂ core have attracted attention as they can be excellent enzyme model systems for the active sites of molybdo-enzymes, such as xanthine oxidase, nitrogenase and sulfite oxidase [15,16].

Accordingly, isothiosemicarbazones would be very good candidates for the synthesis of nickel and molybdenum complexes with various structures and properties, and for extending research in the field of coordination chemistry of isothiosemicarbazone ligands. In this work, we describe the synthesis, spectroscopy, crystal structure and DFT studies of a new isothiosemicarbazone as a free ligand and its molybdenum(VI) and Ni(II) complexes.

* Corresponding authors. Tel./fax: +98 (511) 8975457.
E-mail addresses: rezatakjoo@yahoo.com, r.takjoo@um.ac.ir (R. Takjoo).

2. Experimental

2.1. Materials and instrumentation

All chemicals for the syntheses were obtained from commercial sources. Carbon, hydrogen and nitrogen analyses were performed on a Thermo Finnigan Flash Elemental Analyzer 1112EA. The molar conductance values of the complexes (1.0×10^{-3} M of DMF solutions) were measured by a Metrohm 712 Conductometer. Infrared spectra of KBr pellets were obtained by a FT-IR 8400-SHIMADZU spectrophotometer. ^{1}H NMR spectra in DMSO-d_6 were recorded using a Bruker BRX 100 AVANCE spectrometer. The electronic spectra were carried out in MeOH by a SHIMADZU model 2550 UV–Vis spectrophotometer. Diffraction data were measured using a Bruker APEX II CCD diffractometer.

2.2. Preparation of 3-methoxy-2-hydroxybenzaldehyde S-ethylisothiosemicarbazone (H_2L)

An 10 mL ethanolic suspension of thiosemicarbazide (0.91 g, 10 mmol) and ethyl iodide (1.71 g, 11 mmol) was refluxed in water bath until a colorless solution was obtained. 3-Methoxy-2-hydroxybenzaldehyde (1.52 g, 10 mmol) was added, and refluxing was continued for an extra hour. Finally, a 10 mL aqueous solution of $Na_2CO_3 \cdot 10H_2O$ (5.72 g, 20 mmol) was added to neutralize the hydrogen iodide produced, with constant stirring at room temperature. The neutralization reaction was controlled by pH paper. After cooling, a yellow precipitate was separated, washed several times with cold water and ethanol. Suitable crystals of H_2L were obtained by slow evaporation of its methanolic solution after one week. They were filtered off and dried in vacuo over silica gel.

Yield: 2.1 g (83%). M.p. 138 °C. *Anal.* Calc. for $C_{11}H_{15}N_3O_2S$ (253.32 g mol^{-1}): C, 52.15; H, 5.97; N, 16.59. Found: C, 52.04; H, 5.84; N, 16.67%. IR (KBr) cm^{-1}: $\nu_{asy}(NH_2)$ 3521s; $\nu_{sy}(NH_2)$ 3401 ms; $\nu(OH)$ 3132 m; $\nu(CH)_{aromatic}$ 3020–3097w; $\nu(CH)$–Me, Et 2877–2966w; $\nu(C^7=N^1) + \nu(C=C)$ 1643vs; $\nu(C=C) + \delta_{ipb}(OH) + \delta(NH_2)$ 1601 m; $\nu(C^8=N^2) + \nu(C=C)$ 1512s; $\nu(C=C) + \delta_{ipb}(CH)_{aromatic}$ 1462 m; $\nu(C^1O^1)$ 1242s; $\nu(N^2=C^8-N^3) + \nu(C^2O^2)$ 1210 ms; $\delta_{oopb}(OH)$ 748 m; $\delta_{oopb}(CH)_{aromatic}$ 729 m; $\nu(CSC)$ 623w. ^{1}H NMR (100 MHz, DMSO-d_6) δ: 13 (s, 1H, OH; exchanges with D_2O), 9.7 (s, 2H, NH$_2$; exchanges with D_2O), 8.8 (s, 1H, C^7), 7.6 (d, 1H, C^5), 7.1 (dd, 1H, C^4), 6.8 (d, 1H, C^3), 3.5 (s, 3H, C^{11}), 3.2 (q, 2H, C^9), 1.3 (t, 3H, C^{10}). UV–Vis (methanol) λ_{max} nm (log ε, L mol^{-1} cm^{-1}): 220 (4.75), 306 (4.62), 346 (4.35).

2.3. Preparation of (3-methoxy-2-hydroxybenzaldehyde S-ethyl-isothiosemicarbazonato-N,N′,O)-(1-methylimidazole)-nickel(II) (1)

An ethanolic solution (3 mL) of H_2L (0.25 g, 1 mmol) was added to a 3 mL suspension of Ni(OAC)$_2$·4H$_2$O (0.25 g, 1 mmol) in ethanol. The mixture was stirred at room temperature for 30 min. 1-Methylimidazole (0.08 g, 1 mmol) was then added to the solution and stirring was continued for an extra hour. The clear red solution that formed was left to stand overnight. Suitable crystals of 1 were obtained from the maternal solution. They were filtered off and dried in vacuo over silica gel.

Yield: 0.24 g (62%). M.p. 198 °C. Molar conductivity (1.0×10^{-3} M; DMF): 8 Ω^{-1} cm^2 mol^{-1}. *Anal.* Calc. for $C_{15}H_{19}N_5NiO_2S$ (392.10 g mol^{-1}): C, 45.95; H, 4.88; N, 17.86. Found: C, 45.84; H, 4.74; N, 17.67%. IR (KBr) cm^{-1}: $\nu(NH)$ 3469 m; $\nu(CH)$-1-methylimidazole 3146–3152 m; $\nu(CH)_{aromatic}$ 3062–3112w; $\nu(CH)$–Me, Et 2886–3031w; $\nu(C^7=N^1) + \nu(C=C)$ 1597s; $\nu(C=C) + \delta_{ipb}(NH)$ 1581vs; $\nu(C^8=N^2) + \nu(C=C)$ 1503s; $\nu(C=C) + \delta_{ipb}(CH)_{aromatic}$ 1450s; $\nu(C^1O^1)$ 1233s; $\nu(N^2=C^8-N^3) + \nu(C^2O^2)$ 1218 m; $\delta_{oopb}(CH)_{aromatic}$ 736 m; $\nu(CSC)$ 652w; $\nu(MO)$ 543 m; $\nu(MN)$ 455 m. ^{1}H NMR (100 MHz, DMSO-d_6) δ: 8 (s, 1H, C^7), 7.4–6.8 (m, 6H, C^3, C^4, C^5, C^{12}, C^{13}, C^{14}), 4.2 (s, 1H, NH; exchanges with D_2O), 3.75 (s, 3H, C^{11}), 3.5 (s, 3H, C^{15}), 3 (q, 2H, C^9), 1.3 (t, 3H, C^{10}). UV–Vis (methanol) λ_{max} nm (log ε, L mol^{-1} cm^{-1}): 216 (4.78), 244 (4.62)sh, 302 (4.36), 374 (4.23), 508 (2.36), 560 (2.14).

2.4. Preparation of (3-methoxy-2-hydroxybenzaldehyde S-ethyl-isothiosemicarbazonato-N,N′,O)-(pyridine)-nickel(II) (2)

Ni(OAC)$_2$·4H$_2$O (0.25 g, 1 mmol) and H_2L (0.25 g, 1 mmol) in 10 ml ethanol-pyridine (4:1 ratio) were refluxed for 1 h to give a red solution. After cooling, a red crystalline product precipitated out. The resulting solid was recrystallised in methanol to obtain suitable dark-red single crystals of complex 2 for X-ray diffraction. They were filtered off and dried in vacuo over silica gel.

Yield: 0.21 g (52%). M.p. 176 °C. Molar conductivity (1.0×10^{-3} M; DMF): 9 Ω^{-1} cm^2 mol^{-1}. *Anal.* Calc. for $C_{16}H_{18}N_4NiO_2S$ (389.11 g mol^{-1}): C, 49.39; H, 4.66; N, 14.40. Found: C, 48.84; H, 4.71; N, 14.32%. IR (KBr) cm^{-1}: $\nu(NH)$ 3453 m; $\nu(CH)$-aromatic 3053–3123w; $\nu(CH)$–Me, Et 2889–3024w; $\nu(C^7=N^1) + \nu(C=C)$ 1596s; $\nu(C=C) + \delta_{ipb}(NH)$ 1578 ms; $\nu(C^8=N^2) + \nu(C=C)$ 1504vs; $\nu(C=C) + \delta_{ipb}(CH)$-aromatic 1446s; $\nu(C^1O^1)$ 1242s; $\nu(N^2=C^8-N^3) + \nu(C^2O^2)$ 1218s; $\delta_{oopb}(CH)$-aromatic 740 m; $\nu(CSC)$ 678w; $\nu(MO)$ 554 m; $\nu(MN)$ 446(m). ^{1}H NMR (100 MHz, DMSO-d_6) δ: 8.7 (s, 2H, C^{12}, C^{16}), 8 (s, 1H, C^7), 7.8–6.5 (m, 6H, C^3, C^4, C^5, C^{13}, C^{14}, C^{15}), 4.3 (s, 1H, NH; exchanges with D_2O), 3.6 (s, 3H, C^{11}), 3 (q, 2H, C^9), 1.24 (t, 3H, C^{10}). UV–Vis (methanol) λ_{max} nm (log ε, L mol^{-1} cm^{-1}): 224 (4.83), 248 (4.82)sh, 308 (4.49), 388 (4.43), 512 (2.28), 566 (2.19).

2.5. Cis-dioxo-dimethylsulfoxide-(3-methoxy-2-hydroxybenzaldehyde S-ethyl-isothiosemicarbazonato-N,N′,O)-molybdenum(VI) (3)

3 mL of H_2L (0.25 g, 1 mmol) was added dropwise to a 5 mL methanolic solution of MoO$_2$(acac)$_2$ (0.27 g, 1 mmol) and triethylamine (0.2 g, 2 mmol). The solution mixture was stirred for 2 h. The mixture left to stand overnight. An orange precipitate was separated and washed with cold ethanol. After complete drying, the precipitate was solved in DMSO. The clear solution was placed in a refrigerator. Suitable crystals of 2 were obtained after three days. They were filtered off and dried in vacuo over silica gel.

Yield: 0.34 g (74%). M.p. 190 °C. Molar conductivity (1.0×10^{-3} M; DMF): 12 Ω^{-1} cm^2 mol^{-1}. *Anal.* Calc. for $C_{13}H_{19}MoN_3O_5S_2$ (457.40 g mol^{-1}): C, 34.14; H, 4.19; N, 9.19. Found: C, 34.04; H, 4.24; N, 9.17%. IR (KBr) cm^{-1}: $\nu(NH)$ 3460 m; $\nu(CH)_{aromatic}$ 3044–3093w; $\nu(CH)$–Me, Et 2897–3036w; $\nu(C^7=N^1) + \nu(C=C)$ 1593vs; $\nu(C=C) + \delta_{ipb}(NH)$ 1583s; $\nu(C^8=N^2) + \nu(C=C)$ 1506s; $\nu(C=C) + \delta_{ipb}(CH)_{aromatic}$ 1431 m; $\nu(C^1O^1)$ 1229s; $\nu(N^2=C^8-N^3) + \nu(C^2O^2)$ 1236 m; $\nu_{sy}(cis$-MoO$_2)$ 950s; $\nu_{asy}(cis$-MoO$_2)$ 933s; $\nu(S=O)$-DMSO 902w; $\delta_{oopb}(CH)_{aromatic}$ 733 m; $\nu(CSC)$ 640 m; $\nu(MO)$ 574 m; $\nu(MN)$ 470w. ^{1}H NMR (100 MHz, DMSO-d_6) δ: 8.1 (s, 1H, C^7), 7.4 (d, 1H, C^5), 6.9 (dd, 1H, C^4), 6.6 (d, 1H, C^3), 4.3 (s, 1H, NH; exchanges with D_2O), 3.68 (s, 3H, C^{11}), 3.5 (s, 6H, C^{12}, C^{13}), 3 (q, 2H, C^9), 1.3 (t, 3H, C^{10}). UV–Vis (methanol) λ_{max} nm (log ε, L mol^{-1} cm^{-1}): 218 (4.60), 300 (4.51), 382 (4.08), 450 (3.84).

2.6. X-ray crystal structure determination

X-ray data for the compounds were collected at room temperature with a Bruker APEX II CCD area-detector diffractometer using Mo Kα radiation (λ = 0.71073 Å). Data collection, cell refinement, data reduction and absorption corrections were performed using multiscan methods with Bruker software [17]. The structures were solved by direct methods using SIR2004 [18]. The N-based H atoms and H atoms of OH were found from the difference Fourier map

and refined anisotropically by the full matrix least squares method on F^2 using SHELXL [19]. All the hydrogen (H) atoms were placed at calculated positions and constrained to ride on their parent atoms. The data concerning collection and analysis are reported in Table 1.

3. Computational details

The geometry of the compounds was fully optimized with Density Functional Theory (DFT) using the GAUSSIAN 98 program package [20]. All calculations were carried out with the B3LYP method using the 6-31G* (d,p) basis set for the H, C, N, O and S atoms and Lanl2dz [21,22] basis set for the metal centers in the gas phase. The lack of imaginary frequencies provided evidence for the full optimization of the structures. The Natural Bond Orbital (NBO) analysis has been done with the NBO-code included in Gaussian98 [23].

4. Result and discussion

Four new compounds of **H₂L**, [Ni(L)(1-Me-imidazole)] (**1**), [Ni(L)(pyridine)] (**2**) and [cis-MoO₂(L)DMSO] (**3**) were synthesized. The efforts to achieve suitable crystals for structural analysis were successful. **H₂L** is yellowish and the complexes are red in color. C, H and N analyses were consistent with the proposed structures. The compounds are stable in air and soluble in most common organic solvents, except for H_2O, *n*-hexane and diethyl ether. The molar conductivities of the complexes are 8–12 Ω^{-1} cm² mol⁻¹ in DMF, which proves the neutral behavior of the complexes [8].

Fig. 1. ORTEP drawing of **H₂L** with the atom numbering. Thermal ellipsoids are shown at the 30% probability level.

4.1. Molecular structures

ORTEP views of the compounds with the atom numbering are shown in Figs. 1–4, and related bond distances and inter-bond angles are collected in Table 2. Generally, isothiosemicarbazone organic compounds can be crystallized in *Z* or *E* configurations. In the *Z* isomer, the S–R moiety lies in the *cis* position with respect to the N1 atom, while in the *E* isomer, these moieties lie in *trans* positions with respect to each other. Consistent with the geometries of the isothiosemicarbazone ligands of 2-hydroxybenzaldehyde *S*-methyl isothiosemicarbazone [24], 2-hydroxybenzaldehyde *S*-ethyl isothiosemicarbazone [25] and 2-hydroxybenzaldehyde *S*-allyl isothiosemicarbazone [26], **H₂L** crystallizes as the *Z* isomer. The geometry of **H₂L** is constructed

Table 1
Crystal data and structure refinement for the compounds.

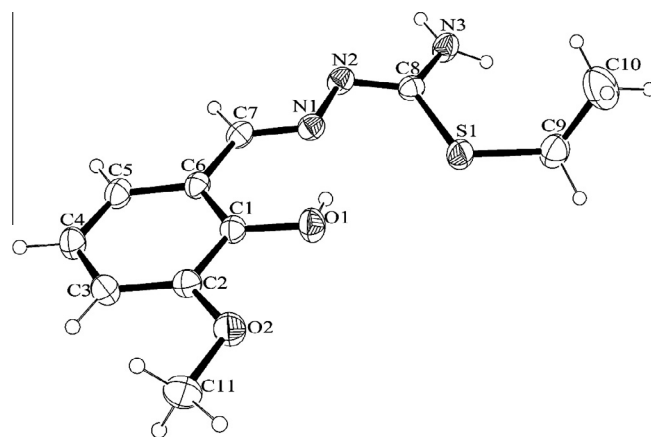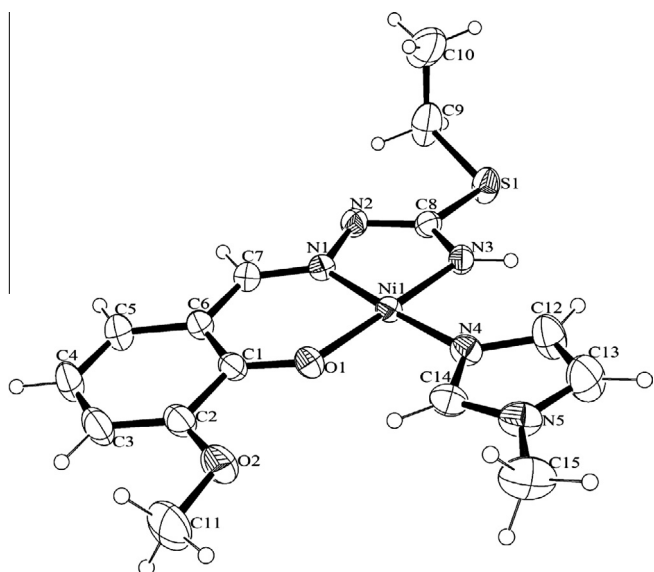| Compound	H₂L	1	2	3
Empirical formula	C₁₁H₁₅N₃O₂S	C₁₅H₁₉N₅NiO₂S	C₁₆H₁₈N₄NiO₂S	C₁₃H₁₉MoN₃O₅S₂
Formula weight	253.32	392.12	389.11	457.37
T (K)	296(2)	296(2)	296(2)	293(2)
Wavelength (Å)	0.71073	0.71073	0.71073	0.71073
Crystal system	monoclinic	monoclinic	monoclinic	triclinic
Space group	P2(1)/n	Cc	P2(1)/c	P1̄
a (Å)	7.5181(2)	9.2511(2)	12.2126(5)	8.0456(8)
b (Å)	12.4704(3)	23.9052(4)	7.4588(3)	9.9751(9)
c (Å)	13.2141(3)	8.9524(2)	19.0638(7)	11.9754(12)
α (°)	90.00	90.00	90	77.048(4)
β (°)	91.2370 (10)	115.5460(10)	103.521(2)	80.407(5)
γ (°)	90.00 (10)	90.00	90	81.920(4)
V (Å³)	1238.58(5)	1786.27(6)	1688.42(12)	918.20(15)
Z,	4	4	4	2
Calculated density (Mg/m³)	1.358	1.458	1.531	1.654
Absorption (mm⁻¹)	0.256	1.220	1.289	0.969
F(000)	536	816	808	464
Crystal size (mm)	0.49 × 0.43 × 0.32	0.44 × 0.32 × 0.18	0.28 × 0.13 × 0.11	0.33 × 0.28 × 0.12
θ (°)	2.25–28	2.58–29.13	1.71–26.99	1.76–27
Limiting indices	−9 ⩽ h ⩽ 9, −16 ⩽ k ⩽ 16, −17 ⩽ l ⩽ 17	−12 ⩽ h ⩽ 12, −32 ⩽ k ⩽ 32, −12 ⩽ l ⩽ 12	−15 ⩽ h ⩽ 15, −9 ⩽ k ⩽ 9, −24 ⩽ l ⩽ 24	−10 ⩽ h ⩽ 10, −12 ⩽ k ⩽ 12, −15 ⩽ l ⩽ 15
Reflections collected/unique (R_int)	25153/2974 (0.0220)	14448/4548 (0.0214)	81280/3698 (0.0283)	24655/3961 (0.0291)
(θ °) Completeness (%)	(28) 99.9	(29.13) 99.6	(26.99) 100.0	(27) 98.9
Refinement method F²	full-matrix least-squares on F²	full-matrix least-squares on F²	full-matrix least-squares on F²	full-matrix least-squares on F²
Data/restraints/parameters	2974/0/166	4548/2/217	3698/2 / 241	3961/1/221
Goodness-of-fit (GOF) on F²	0.989	0.994	1.178	1.071
Final R indices [I > 2σ(I)]	R₁ = 0.0503, wR₂ = 0.1405	R₁ = 0.0215, wR₂ = 0.0597	R1 = 0.0319, wR₂ = 0.0920	R₁ = 0.0197, wR₂ = 0.0538
R indices (all data)	R₁ = 0.0552, wR₂ = 0.1488	R₁ = 0.0231, wR₂ = 0.0608	R₁ = 0.0401, wR₂ = 0.1063	R₁ = 0.0228, wR₂ = 0.0564
Largest difference in peak and hole (e A⁻³)	0.916 and −0.490	0.298 and −0.152	0.635 and −0.343	0.273 and −0.365

Fig. 2. ORTEP drawing of **1** with the atom numbering. Thermal ellipsoids are shown at the 30% probability level.

Fig. 3. ORTEP drawing of **2** with the atom numbering. Thermal ellipsoids are shown at the 30% probability level.
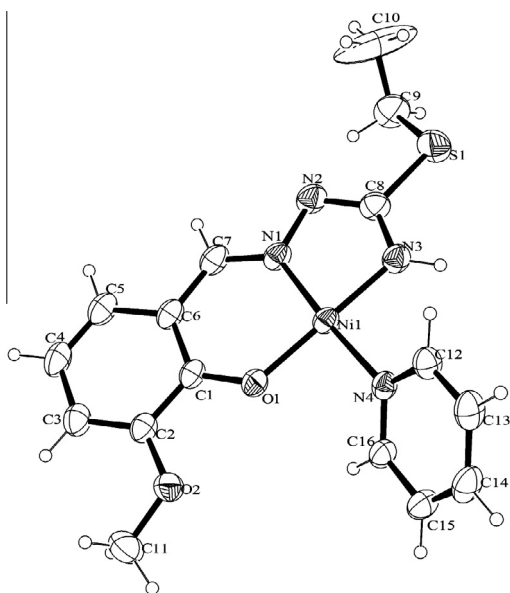

Fig. 4. ORTEP drawing of **3** with the atom numbering. Thermal ellipsoids are shown at the 30% probability level.

by an intramolecular O1–H1···N1 hydrogen bond, with O1–N1 and H1···N1 bond lengths of 2.654(2) and 1.96(3) Å, respectively, and an O–H–N bond angle of 154(3)°. In addition, the intermolecular hydrogen bond of N3–H3B···N2, with the N3–N2 and H3–B···N2 bond distances of 3.095(2) and 2.29(3) Å and an N–H–O bond angle 174(3)°, can join two molecules to form a dimer. The C8–N3 (1.337(2) Å), C8–N2 (1.304(2) Å), N2–N1(1.388(2) Å), N1–C7(1.278(3) Å) and C6–C7(1.449(3) Å) bond distances have the normal values for double and single bond characteristics, which show that π electron delocalization exists through the **H₂L** ligand.

After coordination, the N1–N2, C8–N2 and C7–N1 bond distances in the complexes increase, except for the bond length of C8–N2 in the Mo(VI) complex, which shows no significant change. The C8-N3 bond distance in the Mo(VI) complex increases, while in the Ni(II) complexes it decreases. Although the bond distances in the C7–N1–N2–C8–N3 fragment of the complexes show little
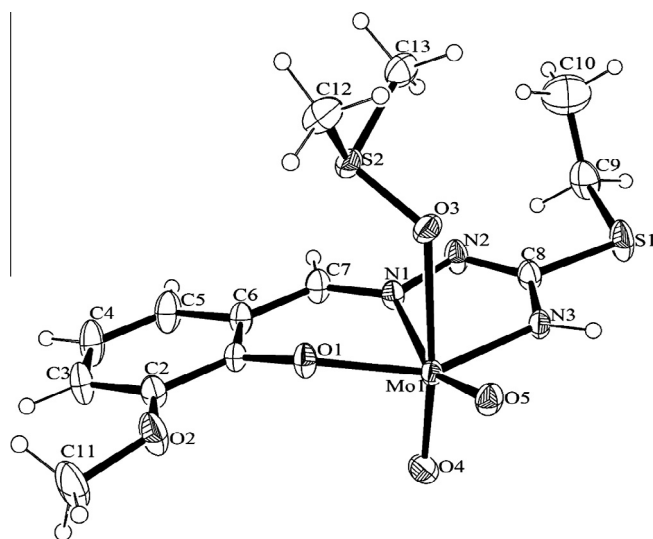
diversity of values with respect to the free **H₂L** ligand, these values still remain in the limits for classical double and single bonds. These are pieces of evidence that the π electron delocalization persists in the deprotonated coordinated ligand in the complexes [27].

On complex formation, the ligand accepts a conformational change from the *Z* isomer to the *E* isomer by rotation of the N3H₂ and *S*-ethyl fragments around the C8–N2 bond. Thereby, the coordination of the ligand through the deprotonated isothioamide nitrogen, azomethine nitrogen and deprotonated oxygen atoms is feasible. In the dibasic form, the ligand is coordinated to the central ions of Ni(II) and Mo(VI) as a tridentate ONN donor agent.

In complexes **1** and **2**, the Ni atoms are located in a distorted square planar fashion, surrounded by the tridentate ONN ligand, with 1-methylimidazole and pyridine, respectively. The Ni1–O1, Ni1–N1, Ni1–N3 and Ni1–N4 bond distances are 1.827(1), 1.837(2), 1.840(1) and 1.916(2) Å for **1** and 1.834(2), 1.835(2), 1.843(2) and 1.911(2) Å in **2**, respectively, which are well comparable with the bond distances found in (benzoylacetone-*S*-methylisothiosemicarbazonato-O,N¹,N⁴)-pyridine-nickel(II) [28] and ammine-(benzoylacetone-*S*-methylisothiosemicarbazonato-N,N′,O)-nickel(II) iodide [29]. The five-membered chelate ring (Ni1–N3–C8–N2–N1) makes a dihedral angle of 3.44° and 2.53° with the adjacent six-membered chelate ring (Ni1–N1–C7–C6–C1–O1) in complexes **1** and **2** respectively, indicating the two chelating rings are approximately planar. The N1–N2–C8–N3 fragment is nearly planar, with a torsion angle of 3.6(2)° and 4.2(3)° in complexes **1** and **2**, as is usually observed in similar Ni(II) complexes of isothiosemicarbazone ligands [30]. The deviations of the Ni(II) atoms in **1** and **2** from the mean plane of O1–N1–N3–N4 are only 0.004 and 0.005 Å respectively, which confirm the planarity of the complexes.

In the complex **3**, the tridentate isothiosemicarbazone ligand is bonded to a *cis*-MoO₂ moiety in a similar approach to the Ni(II) complexes, having a NNO donor set. The sixth position of the octahedral geometry is completed by the oxygen of DMSO, with the weak bond distance of 2.290(1) Å. Accordingly, the molybdenum has a distorted octahedral coordination with the bond angles varying from 70.67(6)° to 104.88(7)°. The two O1 and O2 atoms are *cis* to each other, with a bond angle of 104.88(7)°. This angle is the largest in the coordination sphere, which may be due to the repulsion between the two oxo atoms. The Mo=O4 and Mo=O5 bond

Table 2
Selected experimental (Exp.) and calculated (Calc.) bond distances (Å) and bond angles (°) of the compounds.

| **H₂L** | | | **1** | | | **2** | | **3** | | |
Type	Exp.	Calc.	Type	Exp.	Calc.	Exp.	Calc.	Type	Exp.	Calc.
C8–N3	1.337(2)	1.380	Ni1–O1	1.827(1)	1.857	1.834(2)	1.851	Mo1–O1	1.942(1)	1.991
C8–N2	1.304(2)	1.295	Ni1–N1	1.837(2)	1.872	1.835(2)	1.869	Mo1–N1	2.251(2)	2.307
N2–N1	1.388(2)	1.380	Ni1–N3	1.840(1)	1.874	1.843(2)	1.876	Mo1–N3	2.029(1)	2.055
N1–C7	1.278(3)	1.295	Ni1–N4	1.916(2)	1.959	1.911(2)	1.971	Mo1–O3	2.290(1)	2.499
C6–C7	1.449(3)	1.451	C8–N3	1.321(2)	1.341	1.325(3)	1.344	Mo1–O4	1.701(1)	1.713
C1–O1	1.356(2)	1.343	C8–N2	1.322(2)	1.316	1.316(4)	1.315	Mo1–O5	1.709(2)	1.723
C8–S1	1.762(2)	1.788	N2–N1	1.403(3)	1.387	1.396(3)	1.388	C8–N3	1.345(3)	1.350
C9–S1	1.817(2)	1.844	N1–C7	1.308(2)	1.302	1.301(4)	1.303	C8–N2	1.306(3)	1.312
C6–C7–N1	122.2(2)	122.2	C6–C7	1.431(3)	1.435	1.415(4)	1.433	N2–N1	1.396(2)	1.379
C7–N1–N2	115.5(2)	114.5	C1–O1	1.307(2)	1.306	1.309(2)	1.307	N1–C7	1.291(3)	1.295
N1–N2–C8	112.1(1)	115.2	C8–S1	1.767(2)	1.782	1.762(3)	1.781	C6–C7	1.436(3)	1.448
S1–C8–N3	121.2(1)	118.5	C9–S1	1.799(2)	1.839	1.824(8)	1.839	C1–O1	1.339(2)	1.334
S1–C8–N2	119.4(1)	123.2	N1–Ni1–N4	176.88(8)	177.10	174.63(8)	175.73	C8–S1	1.746(2)	1.773
			O1–Ni1–N3	176.41(6)	176.74	176.21(8)	176.73	C9–S1	1.804(3)	1.839
			O1–Ni1–N1	94.76(7)	94.84	95.57(8)	95.06	S2–O3	1.529(1)	1.542
			N1–Ni1–N3	82.25(7)	82.14	82.51(9)	82.22	O1–Mo1–N3	148.77(6)	143.68
			N3–Ni1–N4	95.75(7)	95.54	93.75(9)	94.68	O5–Mo1–N1	157.76(6)	157.81
			N4–Ni1–O1	87.32(7)	87.49	88.37(7)	88.11	O3–Mo1–O4	170.49(6)	170.69
								O5–Mo1–O4	104.88(7)	106.26
								O4–Mo1–O1	96.30(6)	99.15
								O4–Mo1–N1	93.47(6)	93.43
								O4–Mo1–N3	99.40(7)	102.53
								O3–Mo1–O5	84.47(6)	82.95
								O1–Mo1–O3	78.81(5)	76.61
								N3–Mo1–O3	81.45(6)	77.38
								N1–Mo1–O3	77.82(5)	77.73
								N1–Mo1–N3	70.67(6)	69.85
								S2–O3–Mo1	125.16(8)	121.96

lengths are 1.701(1) and 1.709(2) Å, respectively, exhibiting typical double bond character [31]. The molybdenum atom deviates towards the axial O4 oxygen atom by 0.305 Å from the N1N3O1O5 mean plane. This phenomenon is common in related *cis*-MoO₂ octahedral complexes [10]. The elongation of the Mo1–N1 bond distance is due to the *trans* influence of the O5 oxo atom. The Mo1–O1 and Mo1–N3 bond distances are similar to the values in *cis*-dioxo-dimethylsulfoxide-(2-oxy-1-naphthaldehyde *S*-methylisothiosemicarbazonato N,N′,O)-molybdenum(VI) [32] and *cis*-dioxo-dimethylsulfoxide-(salicylaldehyde *S*-methylisothiosemicarbazonato N,N′,O)-molybdenum(VI) dimethylsulfoxide solvate [33]. The angles between the Mo1–O1–C1–C6–C7–N1 chelate ring and the adjacent Mo1–N3–C8–N2–N1 chelate ring and the aromatic ring are 9.23° and 8.42°, respectively, indicating that the ligand has a slight concave distortion from planarity. Moreover, the N3H···O5 hydrogen bond, with bond distances N3–O5 = 3.037 Å, O5···H = 2.17(1) Å and bond angle NHO = 172(2)°, links the two molecules to each other.

4.2. Geometry optimization

The structures of the compounds were optimized using Density Functional Theory (DFT). Selected calculated bond lengths (Å) and bond angles (°) related to the title compounds are given in Table 2. The parameters resulted from the X-ray crystallography and calculations are analyzed with respect to each other. There is a good agreement between the solid structure and gas phase calculated values, in spite of the small differences between them. This discrepancy is due to the approximate basis set chosen for the calculation. The X-ray crystal diffraction was applied in the solid state, while the calculation was performed in the gas state [34]. The accuracy of the geometry optimization was verified using frequency calculations. No imaginary frequencies were seen, which indicates the minimum global energy of the structures was obtained. Thus, it is possible to use the optimized structures in the frequency and NBO calculations

### 4.3. Electronic charge distribution and NBO analysis

The calculated atomic charges of participating atoms in the bondings are gathered in Table 3. The calculated formal charge values of 0.33, 0.27 and 2.14 a.u. on the central ions for 1, 2 and 3 are smaller than the defined values of +2 and +6 for Ni(II) and Mo(VI). This indicates that the donor atoms transmit electron density to the central metal atoms. According to Table 3, the calculated electron density on the donor atoms of oxygen and nitrogen atoms is less than expected, while the electron density computed on the central ions is more than expected. These observations again confirm electron transmission from the donor atoms towards the central ions [35].

The energy of the HOMO and LUMO orbitals and their orbital energy gap are calculated using the DFT method, and the pictorial illustrations of these frontier orbitals for the compounds are shown in Fig. 5. Positive and negative regions are shown by red and green colors, respectively. The HOMO and LUMO are known as the electron donor and electron acceptor. The energy gap between the HOMO and LUMO characterizes the chemical stability of the molecule. The energy gap in the case of the title compounds **H₂L**, **1**, **2** and **3** are found to be 4.02, 3.71, 3.18 and 3.35 eV, respectively. Since a lower energy gap implies more interaction and less stability, molecule **2** has a higher chemical activity than the other compounds.

The interaction between the HOMO and LUMO enhances the explanation of the first allowed excitation. The HOMO orbital of the complexes is mainly localized on the ligand group. The ligand has 96%, 96% and 99% roles in the HOMO of complexes **1**, **2** and **3**, while in the lowest unoccupied orbital, the ligand has 62%, 57% and 60% electron populations for complexes **1**, **2** and **3**. The LUMO is located on the nickel and molybdenum centers by 38%, 43% and 40% in complexes **1**, **2** and **3** respectively. Accordingly, the transition state from the HOMO to the LUMO in the complexes can be predicted as an admixture of inter-ligand and LMCT charge transfer transitions [36].

Table 3
Charges and electron configurations for the complexes.

1			2			3		
	Charge	Electron configuration		Charge	Electron configuration		Charge	Electron configuration
Ni(1)	0.337830	[core]4S(0.33)3d(8.71)	Ni(1)	0.270741	[core]4S(0.33)3d(8.72)	Mo(1)	2.140478	[core]5S(0.22)4d(3.98)
N(1)	−0.049502	[core]2S(1.32)2p(3.97)	N(1)	−0.004526	[core]2S(1.41)2p(4.00)	N(1)	−0.011394	[core]2S(1.33)2p(3.97)
N(3)	−0.532170	[core]2S(1.41)2p(4.47)	N(3)	−0.85090	[core]2S(1.39)2p(4.44)	N(3)	−0.951724	[core]2S(1.38)2p(4.44)
O(1)	−0.504142	[core]2S(1.68)2p 5.05)	O(1)	−0.66624	[core]2S(1.65)2p(5.00)	O(1)	−0.804147	[core]2S(1.65)2p(5.02)
N(4)	−0.052208	[core]2S(1.36)2p(4.17)	N(4)	−0.080621	[core]2S(1.29)2p(3.95)	O(3)	−0.548697	[core]2S(1.83)2p(5.13)
						O(4)	−0.661319	[core]2S(1.86)2p(4.66)
						O(5)	−0.623768	[core]2S(1.86)2p(4.69)
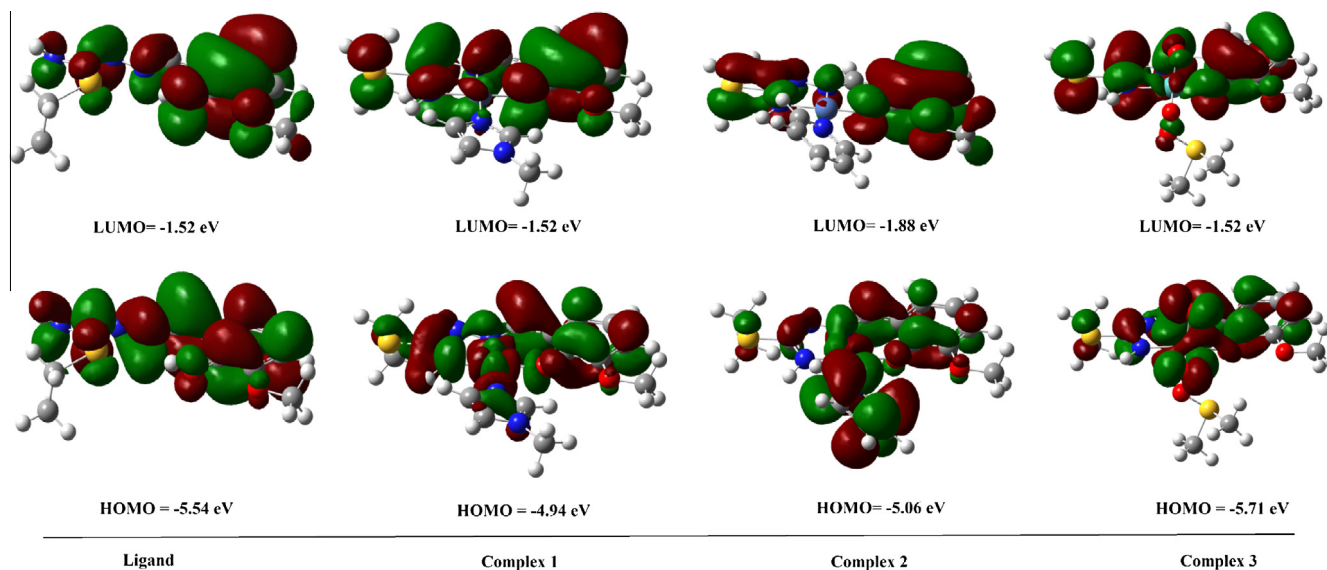
Fig. 5. The HOMO and LUMO views of the compounds.

Table 4
The experimental and calculated IR vibrational frequencies of the free ligand and its Ni(II) and Mo(VI) complexes.

H$_2$L		1		2		3		Assignment
Exp.[a]	Scaled	Exp.	Scaled	Exp.	Scaled	Exp.	Scaled	
–	–	455(m)	476	446(m)	456	470(m)	450	v(MN)
–	–	543(m)	520	554(m)	543	574(m)	565	v(MO)
623(w)	635	652(w)	642	678(w)	654	640(m)	644	v(CSC)
729(m)	712	736(m)	715	740(m)	720	733(m)	762	δ_{oopb}(CH)-aromatic
748(m)	776	–	–	–	–	–	–	δ_{oopb}(OH)
–	–	–	–	–	–	902(w)	912	v(S=O)-DMSO
–	–	–	–	–	–	933(s)	936	v_{asy}(cis-MoO$_2$)
–	–	–	–	–	–	950(s)	954	v_{sy}(cis-MoO$_2$)
1210 ms	1241	1218(m)	1227	1218(s)	1238	1236(m)	1245	v(N^2=C^8–N^3) + v(C^{2}O^2)
1242(s)	1264	1233(s)	1247	1242(s)	1256	1229(s)	1228	v(C^{1}O^1)
1462(m)	1442	1450(s)	1430	1446(s)	1436	1431(m)	1451	v(C = C) + δ_{ipb}(CH)-aromatic
1512(s)	1538	1503(s)	1528	1504(vs)	1532	1506(s)	1524	v(C^8=N^2) + v(C=C)
–	–	1581(vs)	1585	1578(ms)	1583	1583(s)	1581	v(C=C) + δ_{ipb}(NH)
1601(m)	1602	–	–	–	–	–	–	v(C=C) + δ_{ipb}(OH) + δ(NH$_2$)
1643(vs)	1611	1597(s)	1592	1596(s)	1593	1593(vs)	1602	v(C^7=N^1) + v(C=C)
2877–2966(w)	2904–3004	2886–3031(w)	2903–3051	2889–3024(w)	2878–3014(w)	2897–3036(w)	2908–3071	v(CH)-Me, Et
3020–3097(w)	3070–3110	3062–3112(w)	3067–3105	3053–3123(w)	3042–3135(w)	3044–3093(w)	3074–3111	v(CH)-aromatic
–	–	3146–3152(m)	3165–3170	–	–	–	–	v(CH)-1-methylimidazole
3132(m)	3180	–	–	–	–	–	–	v(OH)
3401(ms)	3427	–	–	–	–	–	–	v_{sy}(NH$_2$)
3521(s)	3542	–	–	–	–	–	–	v_{asy}(NH$_2$)
-	-	3469(m)	3480	3453(m)	3476	3460(m)	3484	v(NH)

Abbreviation: vs; very strong, s; strong, m; medium, w; weak, sy; symmetric, asy; asymmetric, v; stretching, δ; bending, oopb; out of plane bending; ipb; in plane bending.
[a] Wavenumbers (cm^{-1}).

4.4. Vibrational assignment

Selected experimental and computed vibrational frequencies and vibrational assignments of **H$_2$L**, **1**, **2** and **3** are given in Table 4.

Generally, the calculated wavenumbers are more than the experimental wavenumbers. It should be considered that the calculation was performed for an isolated molecule in the gas phase, while the experimental values were obtained in the solid state. Therefore,

the calculated values are scaled by a suitable factor, so they can be compared to the experimental wavenumbers much better [37]. In the IR spectrum of **H₂L**, medium absorption bands at 3132 and 748 cm^{-1} are due to stretching and out-of-plane bending vibrations of OH. These bands appear at 3180 and 776 cm^{-1} in the calculated spectrum, respectively. After complexation, the $v(OH)$ and $\delta_{oopb}(OH)$ bands disappear, indicating that the coordination takes place through the deprotonated oxygen atom [10]. The asymmetric and symmetric stretching vibrations of NH_2 are disclosed at 3521 and 3401 cm^{-1} in the experiment, and at 3542 and 3427 cm^{-1} in the calculations [8]. The omission of the stretching vibrations of NH_2 and the appearance of new sharp bands at 3469, 3453 and 3460 cm^{-1} in the infra red spectra of **1**, **2** and **3**, respectively, reveal coordination of the N^3 atom to the metal center [6]. The DFT calculation gives this band at 3480, 3476 and 3484 cm^{-1} for **1**, **2** and **3**, respectively. By the DFT calculations, it can be found that the in-plane-bending vibrations modes of the OH and NH_2 groups mix with the stretching vibration mode of the C=C bonds. This can cause a strong band at 1601 and 1602 cm^{-1} in the experimental and calculated IR spectra of the ligand, respectively. Conversely, in the IR spectra of the complexes, the strong bands at 1581 1578 and 1583 cm^{-1} in the experimental, and at 1585, 1583 and 1581 cm^{-1} in the calculated spectra for 1, 2 and 3, respectively, are assignable to an admixture of the in-plane-bending vibration mode of the NH group with the stretching mode of the C=C bonds [38]. The intense band observed at 1643 cm^{-1}, corresponding to $v(C^7=N^1) + v(C=C)$, is shifted by 46, 47 and 50 cm^{-1} to lower frequencies for complexes **1**, **2** and **3**. The DFT calculation has also confirmed the coordination of the azomethine nitrogen atom by indicating 19, 18 and 9 cm^{-1} displacements to lower frequencies for **1**, **2** and **3**, respectively. This indicates that the azomethine nitrogen atom is bonded to the metallic ions [7]. In the free ligand, the stretching vibration of the C^1O^1 bond at 1242 cm^{-1} exhibits 9, 16 and 13 cm^{-1} displacements to lower frequencies upon complexation, and appears at 1233, 1226 and 1229 cm^{-1} in the IR spectra of complexes **1**, **2** and **3**, respectively [34]. These values are computed at 1264, 1247, 1246 and 1228 cm^{-1} for **H₂L**, **1**, **2** and **3**, respectively. The coordination of the oxygen atom was confirmed by the elimination of the $v(OH)$ band. For the molybdenum(VI) complex, two strong bands at 950 and 933 cm^{-1} are assignable to the symmetric and asymmetric vibrations of the cis-MoO_2 group [32], and the weak band at 902 cm^{-1} demonstrates the coordination behavior of the DMSO molecule [39]. The theoretically scaled values indicate good agreement with the experimentally observed vibrations and disclose $v_{sy}(cis\text{-}MoO_2)$, $v_{asy}(cis\text{-}MoO_2)$ and $v(S=O)$ at 954, 936 and 912 cm^{-1}, respectively.

4.5. UV–Vis spectra

The UV–Vis spectra of the compounds were recorded in methanol, and the detailed data are summarized in Sections 2.2–2.5. The electronic spectrum of **H₂L** shows a $\pi \rightarrow \pi^*$ transition band at 220 nm (4.74). This band shows a blue shift and appears at 216 (4.78), 224 (4.83) and 218 nm (4.60) in the electronic spectra of **1**, **2** and **3** respectively [6]. The $n \rightarrow \pi^*$ transitions of the azomethine and isothioamide fragments are disclosed at 306 (4.62) and 346 nm (4.35) in the spectrum of the free ligand. The spectra of the complexes exhibit only one $n \rightarrow \pi^*$ transitions peak, around 302 (4.36), 308 (4.49) and 300 nm (4.51) for **1**, **2** and **3**, respectively, which may be due to coordination of the azomethine fragment. The bands at 374 nm (4.23) for **1**, 388 nm (4.43) for **2** and two bands at 382 (4.08) and 450 nm (3.84) for **3** can be assigned to N → M and O → M charge transfer transitions. For the square planar Ni(II) complexes, with a d^8 electron configuration and $^1A_{1g}$ ground state, three transitions are possible: $^1A_{1g} \rightarrow {}^1A_{2g}$, $^1A_{1g} \rightarrow {}^1B_{1g}$ and $^1A_{1g} \rightarrow {}^1E_g$. The bands at 560 (2.14) and 508 nm

(2.36) in complex **1** and at 512 (2.28) and 566 nm (2.19) in complex **2** can be attributed to the $^1A_{1g} \rightarrow {}^1A_{2g}$ and $^1A_{1g} \rightarrow {}^1B_{1g}$ transitions, respectively [36]. The third d–d transition was probably covered by the tail of the LMCT charge-transfer absorptions [8]. The molybdenum(VI) complex, with the empty d-orbitals, does not show any d-d transition bands.

4.6. ^1H NMR study

The ^1H NMR spectra of the compounds were recorded in DMSO. The ORTEP diagrams of the compounds can be applied for the assignment of the protons resonances. In the ^1H NMR spectrum of **H₂L**, a singlet signal at 13 ppm is assigned to the OH proton. After coordination, the OH proton resonance disappears, indicating coordination takes place through the deprotonated hydroxyl group. A signal at 9.77 ppm is ascribed to the proton resonance of the NH_2 moiety. A new broad singlet band at about 4.2 ppm appears in the ^1H NMR spectra of the complexes, which is attributed to the N^3H proton. The appearance of this band, with the omission of the NH_2 signal with respect to the free ligand, confirms the coordination of the isothioamide nitrogen atom to the metal centers. The exchangeability of the proton resonances of OH, NH_2 and NH in the ^1H NMR spectra of the compounds has been determined by the addition of D_2O. In the ^1H NMR spectra of the complexes, the azomethine proton resonance shows a significant upfield shift with respect to the free **H₂L** ligand, indicating the N^1 atom is coordinated to the central ions. The signals for the ethyl fragment appear in the same region for **H₂L** and the complexes, which confirms that the sulfur atom does not partake in the complexation. The protons resonances of the aromatic ring and $C^{11}H_3$ occur in the same region for **H₂L** and the complexes. In addition, the C^{12} and C^{13} proton signals at 3.5 ppm in **3** reveal the existence of DMSO as a ligand in the complex.

5. Conclusion

We have synthesized and characterized four new compounds of the isothiosemicarbazone family with the general formulae **H₂L**, [Ni(L)1-Me-imidazole] (**1**), [Ni(L)pyridine] (**2**) and [cis-MoO₂(L)DMSO] (**3**) by the prevailing spectral methods of FT-IR, UV–Vis and ^1H NMR. Their structural features were determined by X-ray crystallographic diffraction. From the structural study, it was concluded that the ligand crystallized as the Z isomer. The ligand coordinated to the metal centers in the similar approach of a tridentate ONN donor. The nickel(II) and molybdenum(VI) centers are assumed to have distorted square planar and octahedral geometries, respectively. The 1-methylimidazole and pyridine ligands occupy the remaining positions of complexes **1** and **2**. The Mo(VI) center is surrounded by L^{-2}, two oxo oxygen atoms and one DMSO solvent. The bond distances in the isothioamide fragment are similar in the ligand and the complexes. This suggests that π electron delocalization persists in this fragment after complexation Finally, some physicochemical properties, like structural parameters and frequency vibrations, obtained from calculations and experimental data were in accordance with each other.

Acknowledgements

Appendix A. Supplementary data

CCDC 898793–898795 and 911676 contains the supplementary crystallographic data for the compounds. These data can be obtained free of charge via http://www.ccdc.cam.ac.uk/conts/retrieving.html, or from the Cambridge Crystallographic Data Centre, 12 Union Road, Cambridge CB2 1EZ, UK; fax: +44 1223 336 033; or e-mail: deposit@ccdc.cam.ac.uk. Supplementary data associated with this article can be found, in the online version, at http://dx.doi.org/10.1016/j.poly.2013.02.078.

References

[1] Y. Qin, R. Xing, S. Liu, K. Li, X. Meng, R. Li, J. Cui, B. Li, P. Li, Carbohydr. Polym. 87 (2012) 2664.
[2] S.A. Reddy, K.J. Reddy, S.L. Narayana, A.V. Reddy, Food Chem. 109 (2008) 654.
[3] M.T. Cocco, C. Congiu, V. Onnis, M.L. Pelleranob, A.D. Logu, Bioorg. Med. Chem. 10 (2002) 501.
[4] A. Plumitallo, M.C. Cardia, S. Distinto, A.D. Logu, E. Maccioni, IL Farmaco 59 (2004) 945.
[5] A.D. Logua, M. Saddi, V. Onnis, C. Sanna, C. Congiu, R. Borgna, M.T. Cocco, Int. J. Antimicrob. Agents 26 (2005) 28.
[6] T. Bal, B. Atasever, Z. Solakoğlu, S. Erdem-Kuruca, B. Ülküseven, Eur. J. Med. Chem. 42 (2007) 161.
[7] R. Yanardag, T.B. Demirci, B. Ülküseven, S. Bolkent, S. Tunali, S. Bolkent, Eur. J. Med. Chem. 44 (2009) 818.
[8] M. Ahmadi, J.T. Mague, A. Akbari, R. Takjoo, Polyhedron 42 (2012) 128.
[9] Y. Kurt, A. Koca, M. Akkurt, B. Ülküseven, Inorg. Chim. Acta 388 (2012) 148.
[10] R. Takjoo, M. Ahmadi, A. Akbari, H. Amiri Rudbari, F. Nicolol, J. Coord. Chem. 65 (2012) 3403.
[11] G.A. Bogdanovic, V.B. Medakovic, L.S. Vojinovic, V.I. Cesljevic, V.M. Leovac, A. Spasojevic-de Bire, S.D. Zaric, Polyhedron 20 (2001) 2231.
[12] (a) S. Rayati, N. Rafiee, A. Wojtczak, Inorg. Chim. Acta 386 (2012) 27;
     (b) M. Volpe, N.C. Mösch-Zanetti, Inorg. Chem. 51 (2012) 1440;
     (c) N.V. Tverdova, E.D. Pelevina, N.I. Giricheva, G.V. Girichev, N.P. Kuzmina, O.V. Kotova, J. Mol. Struct. 1012 (2012) 151;
     (d) A. Biswas, L.K. Das, M.G.B. Drew, G. Aromí, P. Gamez, A. Ghosh, Inorg. Chem. 51 (2012) 7993.
[13] N.H. Khan, N. Pandya, K.J. Prathap, R.I. Kureshy, S.H.R. Abdi, S. Mishra, H.C. Bajaj, Spectrochim. Acta, Part A 81 (2011) 199.
[14] D. Zhang, G.X. Jin, L.H. Weng, F. Wang, Organometallics 23 (2004) 3270.
[15] C.J. Doonan, H.L. Wilson, K.V. Rajagopalan, R.M. Garrett, B. Bennett, R.C. Prince, G.N. George, J. Am. Chem. Soc. 129 (2007) 9421.
[16] A. Magalon, J.G. Fedor, A. Walburger, J.H. Weiner, Coord. Chem. Rev. 255 (2011) 1159.
[17] (a) COSMO, version 1.60, Bruker AXS Inc., Madison, Wisconsin, 2005.;
     (b) SAINT, version 7.06A, Bruker AXS Inc., Madison, Wisconsin, 2005.;
     (c) SADABS, version 2.10, Bruker AXS Inc., Madison, Wisconsin, 2005.
[18] M.C. Burla, R. Caliandro, M. Camalli, B. Carrozzini, G.L. Cascarano, L. De Caro, C. Giacovazzo, G. Polidori, R. Spagna, J. Appl. Crystallogr. 38 (2005) 381.
[19] G.M. Sheldrick, SHELXL97, University of Göttingen, Göttingen, Germany, 1997.
[20] M.J. Frisch et al., GAUSSIAN 98, Revision A.7, Gaussian, Inc., Pittsburgh, PA, 1998.
[21] J.S. Binkley, J.A. Pople, W.J. Hehre, J. Am. Chem. Soc. 102 (1980) 939.
[22] (a) T.H. Dunning, P.J. Hay, H.F. Schaefer, in: Modern Theo. Chem., vol. 3, third ed., Plenum Press, New York, 1976, p. 1.;
     (b) P.J. Hay, W.R. Wadt, J. Chem. Phys. 82 (1985) 299;
     (c) P.J. Hay, W.R. Wadt, J. Chem. Phys. 82 (1985) 270.
[23] E. Reed, L.A. Curtiss, F. Weinhold, Chem. Rev. 88 (1988) 899.
[24] G. Argay, A. Kalman, B. Ribar, V.M. Leovac, A.F. Petrovic, Monatsh. Chem. 114 (1983) 1205.
[25] A.B. Ilyukhin, V.S. Sergienko, V.L. Abramenko, Kristallografiya (Russ.)(Crystallogr. Rep.) 39 (1994) 843.
[26] P.N. Bourosh, M.A. Yampol'skaya, Yu.A. Simonov, N.V. Gerbeleu, S.G. Shova, Zh. Strukt. Khim. (Russ.)(J. Struct. Chem.) 27 (1986) 95.
[27] V.M. Leovac, L.S. Jovanović, V.I. Češljević, LJ. Bjelica, N.J. Ević, Polyhedron 11 (1992) 1029.
[28] G.A. Bogdanovic, A. Spasojevic-de Bire, V.M. Leovac, V.I. Cesljevic, Acta Crystallogr., Sect. C: Cryst. Struct. Commun. 55 (1999) 1656.
[29] N. Galesic, V.M. Leovac, Acta Crystallogr., Sect. C: Cryst. Struct. Commun. 45 (1989) 745.
[30] V.M. Leovac, V.I. Cesljevic, N.V. Gerbeleu, Yu.A. Simonov, A.A. Dvorkin, V.B. Arion, Transition Met. Chem. 18 (1993) 309.
[31] S. Duman, İ. Kızılcıklı, A. Koca, M. Akkurt, B. Ülküseven, Polyhedron 29 (2010) 2924.
[32] Z.D. Tomic, A. Kapor, A. Zmiric, V.M. Leovac, D. Zobel, S.D. Zaric, Inorg. Chim. Acta 360 (2007) 2197.
[33] A.B. Ilyukhin, V.S. Sergienko, V.L. Abramenko, Kristallografiya (Russ.)(Crystallogr. Rep.) 41 (1996) 678.
[34] (a) R. Takjoo, R. Centore, J. Mol. Struct. 1028 (2013) 148;
     (b) R. Takjoo, R. Centore, M. Hakimi, S.A. Beyramabadi, A. Morsali, Inorg. Chim. Acta 371 (2011) 36.
[35] T. Akitsu, Y. Einaga, Polyhedron 24 (2005) 1869.
[36] A. Akbari, M. Ahmadi, R. Takjoo, F.W. Heinemann, J. Coord. Chem. 65 (2012) 4115.
[37] J.P. Merrick, D. Moran, L. Radom, J. Phys. Chem. A 111 (2007) 11683.
[38] D. Lin-Vien, N.B. Colthup, W.G. Fateley, J.G. Grasselli, The Hand Book of Infrared and Raman Characteristic Frequencies of Organic Molecules, Academic Press, Boston, 1991.
[39] V.M. Leovac, E.Z. Iveges, K.M. Szecsenyi, K. Tomor, G. Pokol, S. Gal, J. Therm. Anal. 50 (1997) 431.